Industrial Engineering Journal
ISSN: 0970-2555
Volume : 52, Issue 1, No. 1, January 2023

A MICROGRID BASED ON A WIND DRIVEN DFIG, DG AND SOLAR PV ARRAY FOR OPTIMAL FUEL CONSUMPTION USING THREE LEVEL INVERTER

Chandragiri Radha Charan, Associate professor, Department of Electrical and Electronics Engineering, JNTUH University College of Engineering, Jagtial, Telangana-505501
Amraj Sai charan, M. Tech Student, Department of Electrical and Electronics Engineering, JNTUH University College of Engineering, Jagtial, Telangana-505501: crcharan@jntuh.ac.in ; amrajc106@gmail.com

ABSTRACT
The proposed approach is based on the 3 Level Inverter Control using DC voltage regulator circuit for controlling the machine when wind turbine based converter is connected to grid side of the system. Moreover, a battery energy storage (BES) is connected at same DC bus through a bidirectional buck/boost DC-DC converter to provide path for excess stator power of DFIG. The extraction of maximum power from both wind and solar, is achieved through rotor side VSC control and bidirectional buck/boost DC-DC converter control, respectively. A modified perturb and observe (P&O) algorithm is presented to extract maximum power from a solar PV array. Moreover, the control of load side VSC, is designed to optimize the fuel consumption of DG. A novel generalized concept is used to compute the reference DG power output for optimal fuel consumption. The microgrid is modelled and simulated using SimPowerSystems tool box of MATLAB, for various scenarios such as varying wind speeds, varying insolation, effect of load variation on a bidirectional converter and unbalanced nonlinear load connected at point of common coupling (PCC). The DFIG stator currents and DG currents, are found balanced and sinusoidal.

Keywords : Solar Cell, Three level inverter, RSC Control algorithm, LSC Control algorithm

I. INTRODUCTION:
Power systems currently undergo considerable change in operating requirements mainly as a result of deregulation and due to an increasing amount of distributed energy resources (DER). In many cases DERs include different technologies that allow generation in small scale (microsources) and some of them take advantage of renewable energy resources (RES) such as solar, wind or hydro energy. Having microsources close to the load has the advantage of reducing transmission losses as well as preventing network congestions. The microgrid often psupplies both electricity and heat to the customers by means of combined heat and power plants (CHP), gas turbines, fuel cells, photovoltaic (PV) systems, wind turbines, etc. The energy storage systems usually include batteries and flywheels [2].The storing device in the microgrid is equivalent to the rotating reserve of large generators in the conventional grid which ensures the balance between energy generation and consumption especially during rapid changes in load or generation

From the customer point of view, microgrids deliver both thermal and electricity requirements and in addition improve local reliability, reduce emissions, improve power excellence by supportive voltage and reducing voltage dips and potentially lower costs of energy supply. From the utility viewpoint, application of distributed energy sources can potentially reduce the demand for distribution and transmission facilities. Clearly, distributed generation located close to loads will reduce flows in transmission and distribution circuits with two important effects: loss reduction and ability to potentially substitute for network assets.

Industrial Engineering Journal
ISSN: 0970-2555
Volume : 52, Issue 1, No. 1, January 2023

In addition, the presence of generation close to demand could increase service quality seen by end customers. Microgrids can offer network support during the time of stress by relieving congestions and aiding restoration after faults. The development of microgrids can contribute to the reduction of emissions and the mitigation of climate changes. This is due to the availability and developing technologies for distributed generation units are based on renewable sources and micro sources that are characterized by very low emissions.

II. CONTROL ALGORITHMS OF MICROGRID

The complete description of control algorithms of RSC and LSC, MPPT algorithm of solar PV array, bidirectional buck/boost DC-DC converter, are given in following subsections. A. Control Algorithm for RSC The control algorithm of RSC. The RSC is used to supply the reactive power requirement of DFIG.

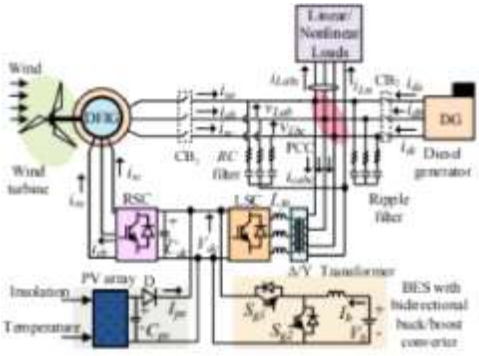

Fig. 1. DFIG based microgrid.

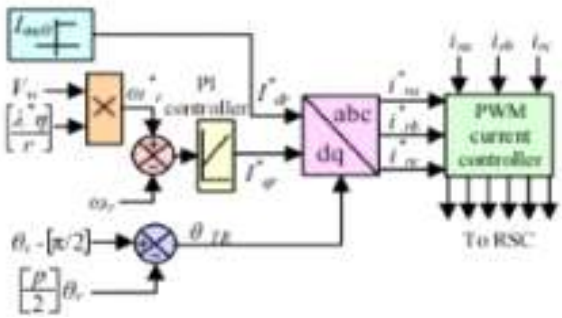

Fig. 2. RSC control algorithm.

and also to regulate the speed for achieving MPPT from the wind turbine. The field oriented vector control (FOVC) is used for RSC to generate the switching pulses. In FOVC, direct axis and quadrature axis components of rotor currents (I * dr, I * qr) represent reactive and active components, respectively. The I * dr is corresponding to no load magnetizing current (Ims0) of DFIG, which is computed as

$$I_{ms0} = \frac{\sqrt{2}V_l}{\sqrt{3}X_m} \quad (1)$$

where Xm denotes the magnetizing reactance of the machine and VL is the line voltage at the machine terminals. The I * qr is estimated by passing the speed error through proportional and integral (PI) controller. and it is derived as,

$$I^*_{qr(k)} = I^*_{qr(k-1)} + K_{p\omega}(\omega_{err(k)} - \omega_{err(k-1)}) + K_{i\omega}\omega_{err(k)} \quad (2)$$

where Kpω and Kiω represent proportional and integral constants of PI speed controller, respectively. The ωerr(k) and ωerr(k-1) denote speed error at kth and (k-1)th instants, respectively. The ωerr(k), is obtained as,

$$\omega_{err(k)} = \omega^*_{r(k)} - \omega_{r(k)} \quad (3)$$

where ω* r(k) and ωr(k) denote the reference and sensed rotor speed of DFIG at kth instant, respectively. The reference rotor speed is obtained from the tip speed ratio MPPT control as,

$$\omega^*_r = \eta\lambda^* V_w / r \quad (4)$$

$$\theta_{2k} = \left(\theta_s - \frac{\pi}{2}\right) - \left(p/2\right)\theta_r \quad (5)$$

where θs is obtained from phase locked loop and θr is computed from the sensed rotor speed as,

Industrial Engineering Journal
ISSN: 0970-2555
Volume : 52, Issue 1, No. 1, January 2023

$$\theta_e = \int_0^t (\omega_e)dt \quad (6)$$

Finally, reference rotor currents (i * ra, i * rb and i * rc) are derived from I * qr and I * dr using an angle of transformation θTR. These reference currents along with sensed rotor currents (ira, irb and irc), are applied to pulse width modulation (PWM) controller to produce RSC gating signals.

Control Algorithm for LSC

The LSC is controlled to achieve the following objectives.

· It maintains the DG and DFIG stator currents sinusoidal and balanced.

· It regulates the DG power within the range of PDmin to PDmax to achieve optimal fuel consumption. Where PDmin and PDmax refer to minimum and maximum DG power output in pu for optimal fuel consumption. A modified indirect vector control based on voltage oriented reference frame, is used to generate the reference currents . In this, both DG and DFIG stator currents are added and controlled to extract maximum power from the DFIG and to regulate the DG power within the range for optimal fuel consumption. The d-axis component of LSC is obtained as,

$$I^*_{dg} = I^*_{dd} + I^*_{dw} \quad (7)$$

where I * dd, I * dw denote the d-component current of DG and DFIG, respectively. It is noted that the saturation block is placed before the I * dd component to operate the DG in optimal fuel efficient zone at change in load. In this work, a generalized concept is used to calculate the DG power based on state of the BES. The reference DG power in pu (P * D) is computed as,

$$P^*_D = P_{D\min} + k_1\beta \quad (8)$$

$$\beta = \frac{V_{b\max} - V_b}{k_2} \quad (9)$$

$$I^*_{dd} = \left(\sqrt{2/3}\right) \times \left(\frac{P^*_D \times VA_{DG}}{V_L}\right) \quad (10)$$

where VL and VADG represent line voltage at PCC and VA rating of DG, which is chosen as a base value. The I * dw is computed as,

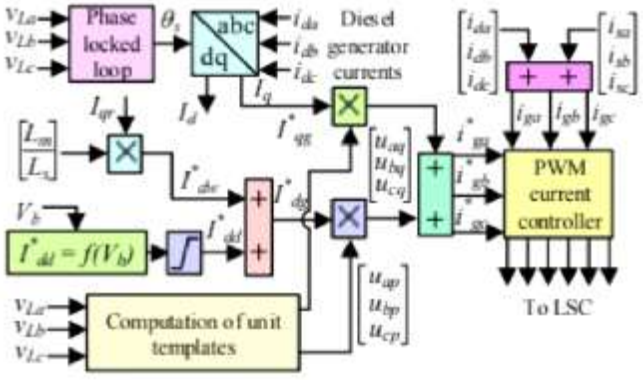

Fig. 3. LSC control algorithm.

$$I^*_{dw} = \left(\frac{L_m}{L_s}\right) I_{qr} \quad (11)$$

The DG currents (ida, idb and idc) are transformed to Id and Iq using angle of transformation (θs), which is obtained from PLL as shown in Fig. 3. The q-axis component of LSC current (I * qg) is

Industrial Engineering Journal
ISSN: 0970-2555
Volume : 52, Issue 1, No. 1, January 2023

numerically same as Iq of DG. The I * dg and I * qg are multiplied with in-phase and quadrature unit templates, respectively and then added together to generate current references (i * ga, i * gb and i * gc). The unit templates are obtained from phase voltages (va, vb and vc). Unit templates of in-phase components are obtained as,

$$u_{ap} = \frac{v_a}{V_m}, u_{bp} = \frac{v_b}{V_m}, u_{cp} = \frac{v_c}{V_m} \Bigg\} \quad (12)$$

Finally, the generated reference currents and sensed current (iga, igb and igc) are applied to PWM controller to produce pulses for LSC.

Where, error of the DC link voltage at kth instant is * V V V de k dc k dc k . Here V * dc(k) and Vdc(k) represent the reference DC link voltage and sensed DC link voltage at kth instant, respectively.

Fig. 4. Control of bidirectional buck or bidirectional boost converter.

Where, error of the battery current at kth instant i * be bk bHere I * b(k) and Ib(k) represent the reference battery current and sensed battery current at kth instant, respectively. The obtained duty ratio (R) is applied to PWM generator to produce pulses for the switches of the bidirectional buck or bidirectional boost converter.

III. Three level - INVERTERS

The execution of the multi-level inverter had been developed and enhanced by utilizing pulse-width-modulation control plan. The utilization of a two-level inverter diminishes the symphonious parts of the yield voltage contrasted and the customary three stage inverter at the same exchanging recurrence. It needs no extra reactors or transformers to diminish the symphonious parts. At that point, it is suitable for medium voltage and medium power frameworks. The outlined and executed two-level inverter understood the necessities and bolstered R-C load by the required estimations of voltage and recurrence

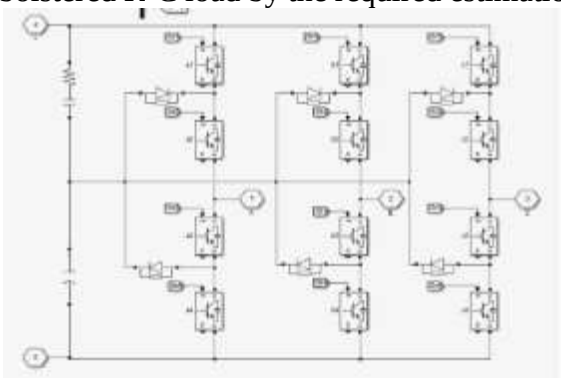

Fig 5: 3 level inverter circuit

For DC-AC conversion, a three-level neutral point clamped multilevel inverter is being used here which is then connected to grid. Multilevel inverters are of basically three types namely three-level neutral point clamped multilevel inverter, cascade H-bridge multilevel inverter and flying-capacitors multilevel inverter. It is very difficult to control the flying-capacitor multilevel inverter compared to a NPC inverter. Additionally, for voltage clamping purpose more number of capacitors are required and for low switching frequency, the required capacitor size should be large. There is separate dc source and non-standard transformer is required as in case of cascade H-bridge multilevel inverter. The quality of output

voltage and output current waveforms is improved in case of three-level NPC inverter. It is having of reduced switching losses and size of output filter is also reduced in this inverter.For DC-AC conversion, a three-level neutral point clamped multilevel inverter is being used here which is then connected to grid. Multilevel inverters are of basically three types namely three-level neutral point clamped multilevel inverter, cascade H-bridge multilevel inverter and flying-capacitors multilevel inverter. It is very difficult to control the flying-capacitor multilevel inverter compared to inverter. Additionally, for voltage clamping purpose more number of capacitors are required and for low switching frequency, the required capacitor size should be large. There is separate dc source and non-standard transformer is required as in case of cascade H-bridge multilevel inverter. The quality of output voltage and output current waveforms is improved in case of three-level NPC inverter. It is having of reduced switching losses and size of output filter is also reduced in this inverter.

For DC-AC conversion, a three-level neutral point clamped multilevel inverter is being used here which is then connected to grid. Multilevel inverters are of basically three types namely three-level neutral point clamped multilevel inverter, cascade H-bridge multilevel inverter and flyingcapacitors multilevel inverter. It is very difficult to control the flying-capacitor multilevel inverter compared to a NPC inverter. Additionally, for voltage clamping purpose more number of capacitors are required and for low switching frequency, the required capacitor size should be large. There is separate dc source and non-standard transformer is required as in case of cascade H-bridge multilevel inverter. The quality of output voltage and output current waveforms is improved in case of three-level inverter. It is having of reduced switching losses and size of output filter is also reduced in this inverter.

To improve the performance of the whole system, this inverter is widely used in rolling mills, variable speed drives and various renewable energy applications

IV. Simulation results

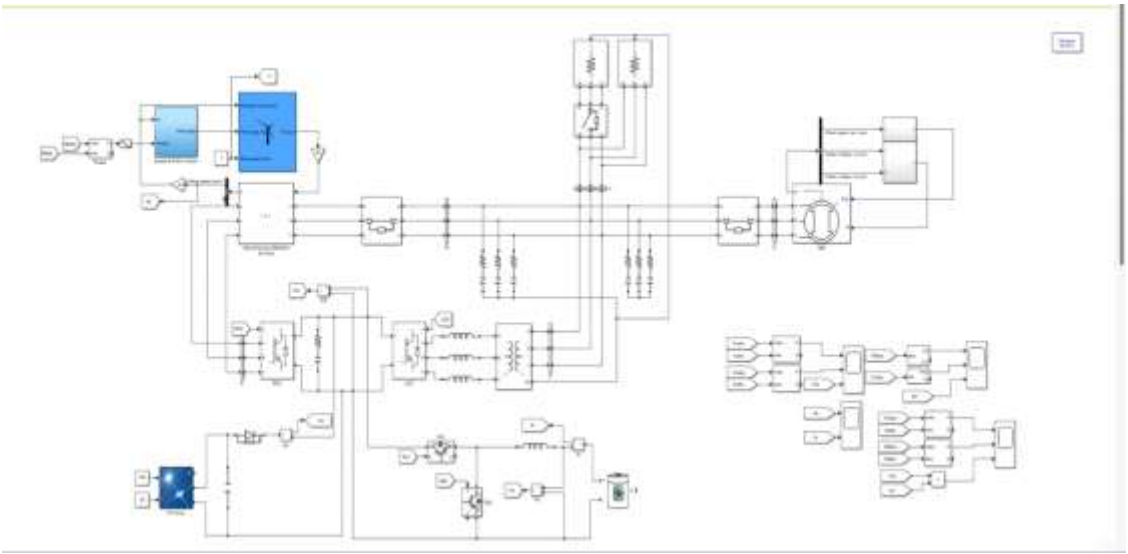

Fig 6 : Simulation circuit

The performance of bidirectional buck or bidirectional boost DC-DC converter at change in the load. The wind speed and insolation are kept at 7 m/s and 700 W/m2 , respectively. Initially a 3-phase balanced load of 2.5 kW is connected at PCC. The DG is delivering 4.84 kW. which corresponds to the battery bank voltage of 125 V. Moreover, the DFIG and solar PV array powers are 2.013 kW and 4.122 kW.

Industrial Engineering Journal
ISSN: 0970-2555
Volume : 52, Issue 1, No. 1, January 2023

Since the total generation is more than the local demand, the remaining power goes to BES through a bidirectional buck/boost DC-DC converter. At t = 3 s, an additional load of 2 kW is connected and again it is disconnected at t = 5.5 s.

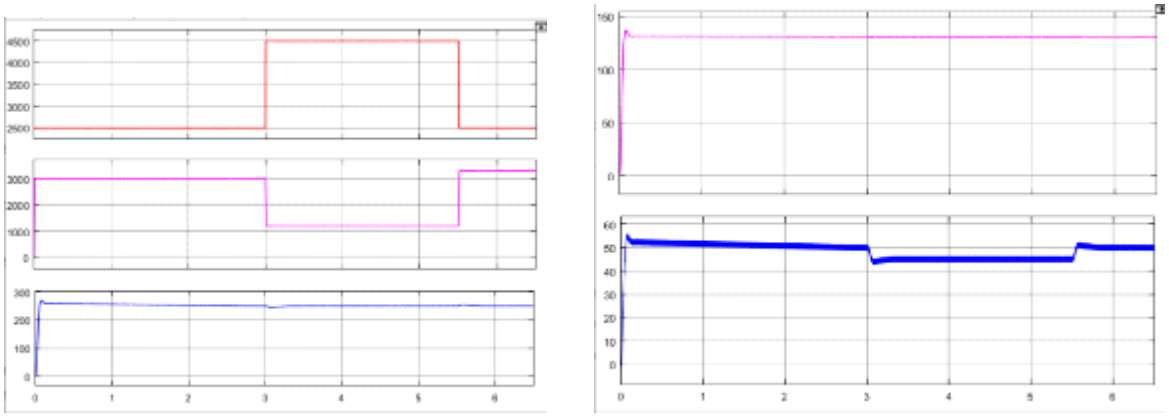

PL, PLSC, Vdc, Ib and Vb

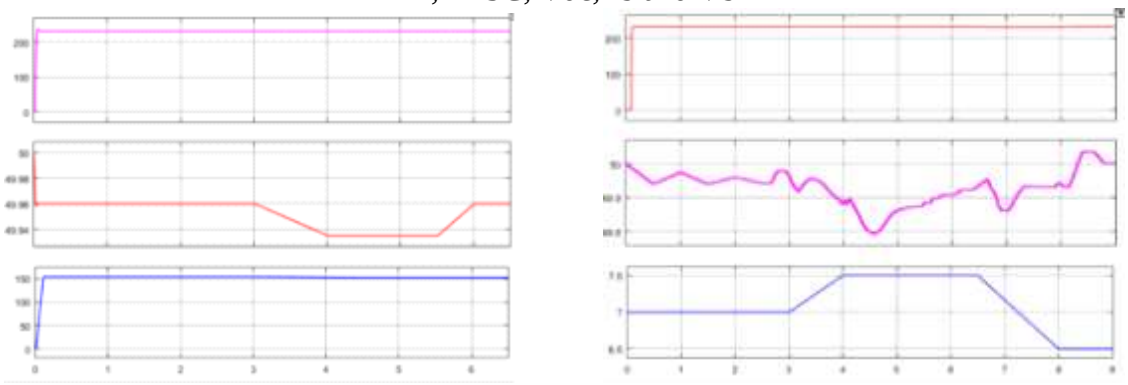

Fig. 7. Performance of bidirectional buck/boost converter at change in (b) Vr, fL, ωr, PD, Pw and Psol

System Performance at Variable Wind Speeds

The performance of the system at variable wind speeds are depicted. In this, a 3-phase load of 4 kW is connected at PCC and the insolation is kept at 700 W/m2. The pattern of wind speed variation is depicted. It is observed that the controller regulates the DFIG rotor speed as per wind MPPT algorithm. Moreover, it is observed that the DC link voltage is regulated. The system dynamic response during the transition of DFIG speed from supersynchronous to subsynchronous speed region, is depicted.

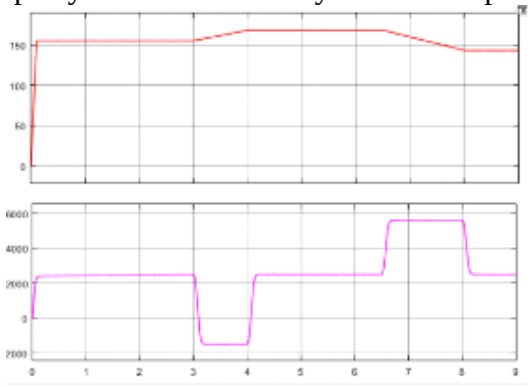

Industrial Engineering Journal
ISSN: 0970-2555
Volume : 52, Issue 1, No. 1, January 2023

Fig. 8. System performance at variable wind speed (a) Vr, fL, Vw, ωr and Pw

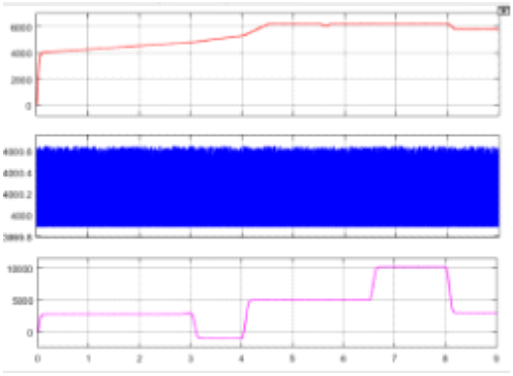

Vdc, Ib, Psol, PD, PL and PLSC.

The DG delivers power of 5.67 kW based on the state of the BES.

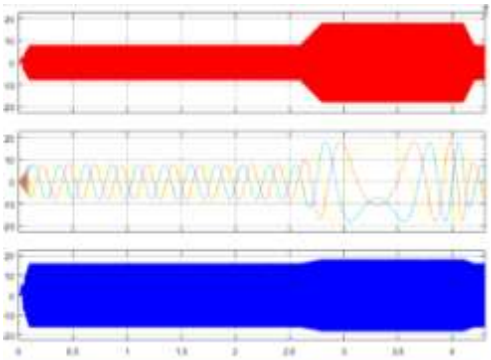

system performance during changeover of DFIG speed from supersynchronous to subsynchronous speed region: Vw, ωr, Cp, isa, irabc and ida.

It is observed that wind MPPT is obtained during the variation of wind speed. Moreover, the frequency rotor currents, is changed according to the speed of operation of DFIG

System Performance at Variable Insolation

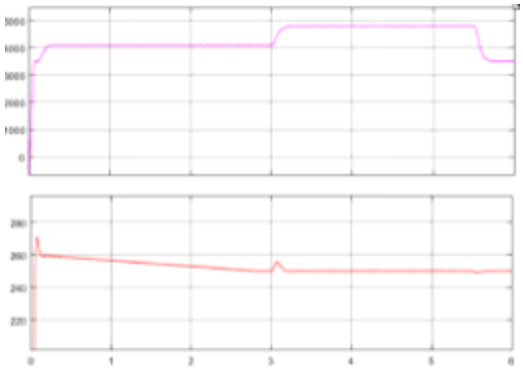

Fig. 9. System performance at variable insolation Vr, ωr, G, Psol and Vdc

The performance of the system at varying solar radiation . In this, the wind speed is kept constant at 7 m/s. Moreover, the DG delivers 4.2 kW power based on the battery voltage. The DC link voltage is

Industrial Engineering Journal
ISSN: 0970-2555
Volume : 52, Issue 1, No. 1, January 2023

regulated by the bidirectional DC-DC converter control for achieving the solar MPPT. Moreover, the solar MPPT is manifested by the Psol waveform.

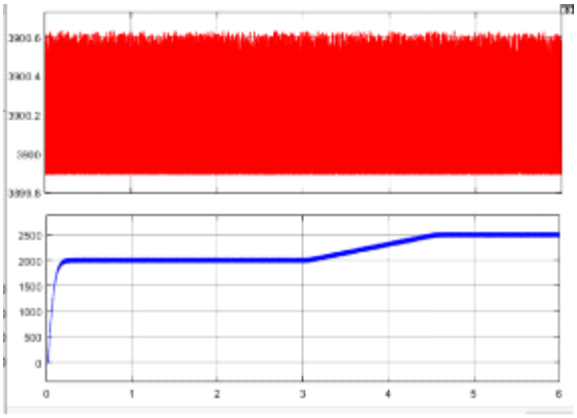

Ib, PD, Pw, PL and PLSC.

In this, a 3-phase linear balanced load of nearly 4 kW is connected at PCC. The insolation of solar PV array is varied from 700 W/m2 to 800 W/m2 at t = 3 s and again it is reduced to 600 W/m2 at t = 5.5 s, as depicted

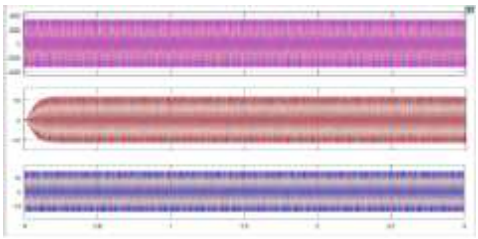

Fig. 10. System voltages and currents at unbalanced nonlinear load: vLabc, isabc, idabc, iLa, iLb, iLc, iLn and icabc.

System Performance at Unbalanced Nonlinear Load The dynamic performance of the system at unbalanced nonlinear load, is depicted in Fig. 10. Initially, a balanced load of 6.7 kW is connected at PCC. It includes a linear load of 0.5 kW and remaining be the nonlinear load, connected on each phase. At t = 2.6 s, a-phase of the load is disconnected and subsequently phase-b, is also disconnected at t = 2.8 s. However, both voltages and currents of DFIG and DG, are maintained balanced and follow the IEEE 519 standard. The LSC helps in unbalance and harmonics compensation of the connected load at PCC. The LSC currents and neutral current. Moreover, the variation of power at unbalanced nonlinear load

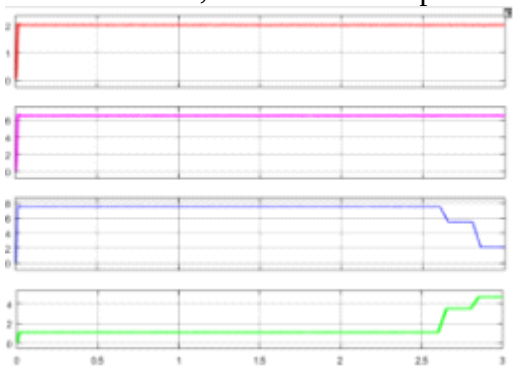

Fig. 11. System performance at nonlinear unbalanced load: Vr, Vdc, Ib, Psol, Pw, PD, PL and PLSC.

It demonstrates waveforms of Vr, Vdc, Ib, Psol, Pw, PD, PL and PLSC. From these results, it is observed that the DC link voltage is regulated and moreover, solar PV and wind MPPT operation is unaffected. The decrease in load power goes to BES through LSC, which is evident from Ib, PL and PLSC waveforms. Moreover, Vr is maintained at constant value.

V. CONCLUSION

In this paper, 3- level inverter control technique for wind turbine was studies. In order to further validate this technique, the method is applied to a wind energy conversion system and the simulation results show improved performance. In addition, the high dynamic performances of the DC voltage regulator control method for 3-level inverter were also illustrated.

The microgrid based on wind turbine driven DFIG, DG and solar PV array with BES, with minimum number of converters, has been presented. The solar PV array is directly connected to DC link of back-back connected VSCs, whereas BES is connected through a bidirectional buck/boost DC-DC converter. The system has been simulated for various scenarios such as variable wind speeds, variable insolation and unbalanced nonlinear load connected at PCC. Moreover, the performance of bidirectional buck/boost DC-DC converter at change in the load has been investigated. Simulated results have shown the satisfactory performance of the system to achieve optimal fuel consumption. The DFIG stator voltages, currents and DG currents, are found balanced and sinusoidal.

Scope of future work

a. The modeling and control can be done for the islanded mode of operation.
b. The control mechanism can be developed for a microgrid containing unbalanced and nonlinear loads.

REFERENCES

[1] J. Knudsen, J. D. Bendtsen, P. Andersen, K. K. Madsen, and C. H. Sterregaard, “Supervisory control implementation on diesel-driven generator sets,” IEEE Trans. Ind. Electron., vol. 65, no. 12, pp. 9698- 9705, Dec. 2018.

[2] J. Jo, H. An, and H. Cha, “Stability improvement of current control by voltage feedforward considering a large synchronous inductance of a diesel generator,” IEEE Trans. Ind. Applicat., vol. 54, no. 5, pp. 5134- 5142, Sept.-Oct. 2018.

[3] Y. Zhang, A. M. Melin, S. M. Djouadi, M. M. Olama and K. Tomsovic, “Provision for guaranteed inertial response in diesel-wind systems via model reference control,” IEEE Trans. Power Systems, vol. 33, no. 6, pp. 6557-6568, Nov. 2018.

[4] N. Nguyen-Hong, H. Nguyen-Duc, and Y. Nakanishi, “Optimal sizing of energy storage devices in isolated wind-diesel systems considering load growth uncertainty,” IEEE Trans. Ind. Applicat., vol. 54, no. 3, pp. 1983-1991, May-June 2018.

[5] W. Li, P. Chao, X. Liang, J. Ma, D. Xu, and X. Jin, “A practical equivalent method for DFIG wind farms,” IEEE Trans. Sustain. Energy, vol. 9, no. 2, pp. 610-620, April 2018.

[6] T. Adefarati, R. C. Bansal, and J. John Justo, “Techno-economic analysis of a PV–wind–battery–diesel standalone power system in a remote area,” The Journal of Engineering, vol. 2017, no. 13, pp. 740- 744, 2017.

[7] C. Wu and H. Nian, “Stator harmonic currents suppression for DFIG based on feed-forward regulator under distorted grid voltage,” IEEE Trans. Power Electron., vol. 33, no. 2, pp. 1211-1224, Feb. 2018.

[8] N. K. Swami Naidu and B. Singh, “Experimental implementation of doubly fed induction generator-based standalone wind energy conversion system,” IEEE Trans. Ind. Applicat., vol. 52, no. 4, pp. 3332- 3339, July-Aug. 2016.